

EFFECT OF GEOMETRY OF STENOSIS ON THE COMPUTATION OF FLOW CHARACTERISTICS OF UNSTEADY BLOOD FLOW IN A COLLAPSIBLE VESSEL

Aik Ying Tang^a, Mohd Al-Akhbar Mohd Noor^b, Airil Yasreen Mohd Yassin^c, Norsarahaida Saidina Amin^{a,d*}, Mohd Zhafri Jamil Abd Nazir^b

^aDepartment of Mathematical Sciences, Faculty of Science, Universiti Teknologi Malaysia, 81310 UTM Johor Bahru, Johor, Malaysia

^bFaculty of Civil Engineering, Universiti Teknologi Malaysia, 81310 UTM Johor Bahru, Johor, Malaysia

^cSchool of Energy, Geoscience, Infrastructure and Society, Heriot-Watt University Malaysia, 62200 Putrajaya, Malaysia

^dDepartemen Matematika, Fakultas Sains dan Teknologi, Universitas Airlangga, East Java 60115, Indonesia

Article history

Received

26 May 2019

Received in revised form

8 December 2020

Accepted

20 December 2020

Published online

23 February 2021

*Corresponding author
norsarahaida@utm.my

Abstract

This paper discusses the effect of different geometric representations of stenosis on the numerical solution of one-dimensional unsteady blood flow in stenotic blood vessel (or stenosis) taking into account fluid-structure interaction. In the formulation, a collapsible pressure-area constitutive relation is added to the coupled mass and momentum equations to allow for the interaction between the cross sectional area, volumetric flow rate and pressure of the flow and hence the prevalence of the one-dimensional fluid-structure interaction. The formulation is stabilized by employing Streamline-Upwind Petrov-Galerkin scheme. Non-reflecting boundary conditions are imposed based on the method of characteristics. Flow characteristics and the geometrical effects of the stenosis are then discussed. Numerical results show that stenosis with irregular shape is more prone to collapse as compared to the smooth one for a given baseline conditions. This study, thus, highlights the importance of representing the shape of the stenosis as close as possible as it might give information otherwise missing in the simplistic smooth representation of the stenosis.

Keywords: Blood flow, streamline-upwind Petrov-Galerkin, stenosis, vessel collapse, fluid-structure interaction

Abstrak

Kajian ini membincangkan kesan bentuk geometri stenosis ke atas penyelesaian berangka aliran darah tak mantap di dalam pembuluh darah berbentuk stenotik. Formulasi yang diterbitkan menggunakan persamaan hubungan antara tekanan dan luas permukaan boleh-runtuh untuk melengkapkan persamaan-persamaan jisim dan momentum bagi membolehkan interaksi wujud di antara luas permukaan, kadar aliran isipadu dan tekanan dalam menghasilkan interaksi-bendalir-struktur satu dimensi. Formulasi ini telah distabilkan menggunakan skema *Streamline-Upwind-Petrov-Galerkin*. Keadaan sempadan tidak memantul digunakan mengikut kaedah ciri. Perbincangan mengenai aliran ciri dan kesan geometri stenosis ke atas aliran darah telah dibuat secara mendalam. Hasil keputusan berangka menunjukkan stenosis berbentuk tidak sekata lebih senang untuk runtuh berbanding stenosis yang licin dan sekata pada garis asas yang sama. Kajian ini seterusnya menegaskan kepentingan mewakili bentuk stenosis dengan ketepatan tinggi bagi mengelakkan kehilangan maklumat seandainya persamaan bentuk stenosis yang kurang tepat digunakan.

Kata kunci: aliran darah, *Streamline-Upwind-Petrov-Galerkin*, stenosis, keruntuhan salur pembuluh, interaksi-bendalir-struktur

© 2021 Penerbit UTM Press. All rights reserved

1.0 INTRODUCTION

Numerical modelling of blood flow has been shown able to provide key information for hemodynamic non-intrusive monitoring. While the problem is effectively three dimensional (3D), one-dimensional (1D) models have been shown as being adequate in capturing the dominant effects at less computational cost [1, 2, 14-22]. This, thus, motivates the study of one-dimensional modelling despite its mathematical simplicity.

One-dimensional fluid-structure-interaction (1D-FSI) blood flow problem is governed by the mass and the linear momentum equations as well as the pressure-area constitutive relation. Such coupling allows the interaction between cross sectional area, A , volumetric flow rate, Q and pressure of the flow, P . Various forms of pressure-area constitutive relation have been proposed in literature [1-7]. Generally, it can be given as

$$P - P_e = f(A) \quad (1)$$

where P_e is the external pressures and $f(A)$ highlights the dependency of the pressure's magnitude on the distribution of the cross-sectional area of the flow. The pressure difference (i.e. $P - P_e$) is termed as transmural pressure.

Although the governing equations are simple, analytical solutions are not available thus it is common to solve the problem numerically [1-7]. In recent works by Sochi [5, 6], Bubnov-Galerkin finite element was formulated where good verifications of results were reported despite no stabilization scheme was employed. However, in our recent work [8], we showed that Sochi's formulation produced spurious oscillations when repeated for higher pressure gradient cases. In accordance, we have proposed a stabilized formulation employing Streamline-Upwind Petrov-Galerkin (SUPG) in that work.

Herein, we extend our work to unsteady problems. We also consider geometrical variation of the vessel to represent stenosis. This is motivated by the question whether smooth representation of the shape of the stenosis is sufficient to render important information of the blood flow. This question has been considered in higher dimensions modelling (2D or 3D), with or without fluid-structure-interaction [9-13]. In the studies carried out by our fourth author on multi-irregular stenosis [12, 13], it was shown that solutions are sensitive to the shape of the stenosis. However, despite the availability in 2D and 3D models, 1D-FSI studies on the subject are still limited. Pioneering studies of [2-4] only considered smooth stenosis. No stenosis was considered in [1, 5, 6]. It is therefore of great interest to consider such a question when in many occasions, the less-consuming one dimensional modelling has been the preferred approach for the analysis. Furthermore, our work is the first to employ SUPG finite element formulation to the problem.

In our formulation, we employ first-order forward difference for the time integration and use Newton-Raphson technique as the nonlinear scheme. The imposition of the non-reflecting boundary conditions is performed by replacing the mass equation with compatibility condition at the boundary nodes. The numerical results are verified against data available in literature. The effect of the geometry of the stenosis to the flow characteristics and vessel collapse phenomenon are then discussed. Since our discussion revolves around the collapse phenomenon of the blood vessel, it is prompt to give its definition at the onset. Collapse of vessel is defined as the point when the vessel area becomes reduced from its normal (initial) condition with a corresponding change from positive to negative pressure of the flow [2].

2.0 METHODOLOGY

2.1 Governing Equations

Unsteady blood flow in stenotic vessel is governed by the mass and the momentum equations complemented by the pressure-area constitutive relation. The corresponding governing equations with frictional losses as detailed in [2, 3] are given as

$$\frac{\partial A}{\partial t} + \frac{\partial Q}{\partial x} = 0 \quad (2)$$

$$\frac{\partial Q}{\partial t} + \frac{\partial}{\partial x} \left(\frac{Q^2}{A} \right) + \frac{A}{\rho} \frac{\partial (P - P_e)}{\partial x} + F_{\text{frict}} A = 0 \quad (3)$$

$$P - P_e = K_p \left[\left(\frac{A}{A_o} \right)^{n_1} - \left(\frac{A}{A_o} \right)^{-n_2} \right] \quad (4)$$

where t is time, x is the axial coordinate along the vessel, ρ is the fluid density, K_p is the tube stiffness and A_o is the no-flow cross sectional area of the flow. n_1 and n_2 are the tube law exponent parameters obtained from experimental data for a bovine carotid artery [2]. F_{frict} is a lumped frictional loss introduced in [3] to account for the viscous losses due to friction between the blood vessel and the fluid as an enhancement to the otherwise inviscid flow of an earlier work [4]. It is defined as

$$F_{\text{frict}} = \begin{cases} \frac{32\mu f_L}{\rho D_e^2} \left(\frac{Q}{A} \right), & \text{Laminar loss} \\ \frac{K_{\text{sep}}}{2} \left(\frac{1}{A_{th}} \right)^2 \frac{Q^2}{L_s}, & \text{Separation loss} \end{cases} \quad (5)$$

where μ is the fluid viscosity, f_L is the major laminar loss coefficient, K_{sep} is the separation loss coefficient, A_{th} is the throat cross sectional area of the stenosis, x_{sep} and L_s are the separation point and length of separation region of the stenosis. D_e is the hydraulic diameter used to account for the noncircular shape of the compressed vessel for the negative transmural pressures where,

$$D_e = \begin{cases} \left(\frac{A}{A_o}\right) D_0, & \frac{A}{A_o} < 1 \\ D_0, & \frac{A}{A_o} \geq 1 \end{cases} \quad (6)$$

For the stenosis model, the cross sectional area and the stiffness variations along the vessel are defined by sine functions as:

$$A_o(x) = A_{oo}\lambda_A(x) \quad (7)$$

$$K_p(x) = K_{p_o}\lambda_K(x) \quad (8)$$

where A_{oo} and K_{p_o} are the nominal vessel cross sectional area and the nominal vessel stiffness, respectively. λ_A and λ_K are the stenosis shape function and the stiffness variation function, respectively.

2.2 Numerical Method

The governing equations given by equation (2) and equation (3) is written in vector form for numerical implementation convenience as follows in which equation (3) is expanded with the insertion of equation (4).

$$\frac{\partial \mathbf{U}}{\partial t} + \frac{\partial \mathbf{F}}{\partial x} + \mathbf{B} = 0 \quad (9)$$

where

$$\mathbf{U} = \begin{bmatrix} A \\ Q \end{bmatrix} \quad (10)$$

$$\mathbf{F} = \begin{bmatrix} Q \\ \frac{Q^2}{A} + \frac{K_p A}{\rho} \left[\frac{\left(\frac{A}{A_o}\right)^{n_1} n_1}{n_1 + 1} - \frac{\left(\frac{A}{A_o}\right)^{-n_2} n_2}{n_2 - 1} \right] \end{bmatrix} \quad (11)$$

$$\mathbf{B} = \begin{bmatrix} 0 \\ K_1 \frac{\partial A_o}{\partial x} + K_2 \frac{\partial K_p}{\partial x} + F_{\text{frict}} A \end{bmatrix} \quad (12)$$

and

$$K_1 = \frac{K_p A}{\rho A_o} \left[-\left(\frac{A}{A_o}\right)^{n_1} n_1 - \left(\frac{A}{A_o}\right)^{-n_2} n_2 + \frac{\left(\frac{A}{A_o}\right)^{n_1} n_1^2}{n_1 + 1} + \frac{\left(\frac{A}{A_o}\right)^{-n_2} n_2^2}{n_2 - 1} \right] \quad (13)$$

$$K_2 = \frac{A}{\rho} \left[\left(\frac{A}{A_o}\right)^{n_1} - \left(\frac{A}{A_o}\right)^{-n_2} - \frac{\left(\frac{A}{A_o}\right)^{n_1} n_1}{n_1 + 1} + \frac{\left(\frac{A}{A_o}\right)^{-n_2} n_2}{n_2 - 1} \right] \quad (14)$$

2.2.1 Weak Statement – SUPG Formulation

The SUPG weak statement for the problem is established by employing integration by parts to equation (9) and inserting a stabilizing term. It is given as follows.

$$\int_x \mathbf{w} \cdot \frac{\partial \mathbf{U}}{\partial t} dx + \int_x \left[-\left(\frac{\partial \mathbf{w}}{\partial x}\right) \cdot \mathbf{F} + \mathbf{w} \cdot \mathbf{B} \right] dx + \int_x (\mathbf{P}(\mathbf{w}) \tau \mathbf{R}(\mathbf{U})) dx + [\mathbf{w} \cdot \mathbf{F}] \Big|_{x=0}^{x=L} = 0 \quad (15)$$

where $\mathbf{P}(\mathbf{w})$ is the operator applied to the weighting function, \mathbf{w} , $\mathbf{R}(\mathbf{U})$ is the residual of the governing equation in quasi-linear form and τ is the stabilization parameter, all as detailed in [23, 24]. Terms in equation (15) are given as

$$\mathbf{P}(\mathbf{w}) = \mathbf{H} \frac{\partial \mathbf{w}}{\partial x} \quad (16)$$

$$\mathbf{R}(\mathbf{U}) = \mathbf{H} \frac{\partial \mathbf{U}}{\partial x} + \mathbf{S} \quad (17)$$

$$\tau = (\mathbf{b}\mathbf{b})^{-\frac{1}{2}} \quad (18)$$

$$\mathbf{b} = \frac{\partial \xi}{\partial x} \mathbf{H} \quad (19)$$

$$\mathbf{H} = \frac{\partial \mathbf{F}}{\partial \mathbf{U}} = \begin{bmatrix} 0 & 1 \\ -\frac{Q^2}{A^2} + \frac{K_p}{\rho} \left[\left(\frac{A}{A_o}\right)^{n_1} n_1 + \left(\frac{A}{A_o}\right)^{-n_2} n_2 \right] & \frac{2Q}{A} \end{bmatrix} \quad (20)$$

$$\mathbf{S} = \begin{bmatrix} 0 & 0 \\ \frac{K_p}{\rho A_o} \left[-\left(\frac{A}{A_o}\right)^{n_1} n_1 - \left(\frac{A}{A_o}\right)^{-n_2} n_2 \right] \frac{\partial A_o}{\partial x} & F_{\text{frict}} \end{bmatrix} + \begin{bmatrix} 0 & 0 \\ \frac{1}{\rho} \left[\left(\frac{A}{A_o}\right)^{n_1} - \left(\frac{A}{A_o}\right)^{-n_2} \right] \frac{\partial K_p}{\partial x} & 0 \end{bmatrix} \quad (21)$$

where $x = x(\xi)$ is the actual coordinates whilst ξ refers to normalized local coordinates. To note, the weighting function \mathbf{w} in equation (15) is the same as the shape functions used for the variable interpolations, given as

$$A = \sum_i^n N_i A_i \quad (22)$$

$$Q = \sum_i^n N_i Q_i \quad (23)$$

where N_i is the i^{th} linear shape function.

2.2.2 Time Integration and Nonlinear Scheme

The hyperbolic nature of the governing equations allows time marching scheme to be employed. Time derivative term in equation (15) is expanded by first order forward difference as

$$\frac{\partial \mathbf{U}}{\partial t} \approx \frac{\mathbf{U}^{t+\Delta t} - \mathbf{U}^t}{\Delta t} \quad (24)$$

where time step, Δt is chosen in such a way it satisfies the Courant–Friedrichs–Lewy (CFL) condition. For the implementation of the Newton-Raphson scheme, equation (22) to (24) are inserted into equation (15) to give the residual function, \mathbf{R}_f (in explicit form) as

$$\mathbf{R}_f = \mathbf{M} \frac{\mathbf{U}^{t+\Delta t} - \mathbf{U}^t}{\Delta t} + \mathbf{K}\mathbf{U}^t \quad (25)$$

where \mathbf{M} and \mathbf{K} are the mass and the stiffness matrices, respectively. Expanding equation (25) about the r^{th} known iteration gives

$$\mathbf{R}_f^r + \frac{\partial \mathbf{R}_f^r}{\partial \mathbf{U}^r} \Delta \mathbf{U} = \mathbf{0} \quad (26)$$

Rearranging gives

$$\mathbf{T}\Delta \mathbf{U} = -\mathbf{R}_f^r \quad (27)$$

where \mathbf{T} is the tangent stiffness matrix. The $r+1$ solution is then obtained by updating the previous solution as follows

$$\mathbf{U}^{r+1} = \Delta \mathbf{U} + \mathbf{U}^r \quad (28)$$

The iteration continues until a convergence criterion is met.

2.2.3 Imposition of Boundary Conditions

The weak formulation in equation (15) is prescribed with suitable boundary conditions in the form of compatibility conditions. Based on the method of characteristics as detailed in [5-7, 16-17], the eigenvalues of \mathbf{H} can be obtained by solving

$$\det(\mathbf{H} - \lambda \mathbf{I}) = 0 \quad (29)$$

where λ is the vector of the eigenvalues and \mathbf{I} is the identity matrix. Left-eigenvectors, \mathbf{L} can be obtained by solving

$$\mathbf{L}\mathbf{H} = \mathbf{L}\mathbf{\Lambda} \quad (30)$$

where \mathbf{L} is left the eigenvectors of \mathbf{H} whilst $\mathbf{\Lambda}$ is given as

$$\mathbf{\Lambda} = \begin{bmatrix} \lambda_1 & 0 \\ 0 & \lambda_2 \end{bmatrix} \quad (31)$$

By solving equation (30) and equation (31), the eigenvalues and the left-eigenvectors are given as

$$\lambda_{1,2} = \frac{Q}{A} \pm \sqrt{\frac{K_p}{\rho} \left[\left(\frac{A}{A_0}\right)^{n_1} n_1 + \left(\frac{A}{A_0}\right)^{-n_2} n_2 \right]} \quad (32)$$

$$\mathbf{L}_{1,2} = \begin{bmatrix} -\frac{Q}{A} \pm \sqrt{\frac{K_p}{\rho} \left[\left(\frac{A}{A_0}\right)^{n_1} n_1 + \left(\frac{A}{A_0}\right)^{-n_2} n_2 \right]} & 1 \end{bmatrix} \quad (33)$$

Specifically for the imposition of the boundary conditions, equation (9) is rearranged in quasi-linear form by employing chain rule and inserting equation (21) in place of \mathbf{B} , thus;

$$\frac{\partial \mathbf{U}}{\partial t} + \mathbf{H} \frac{\partial \mathbf{U}}{\partial x} + \mathbf{S} = \mathbf{0} \quad (34)$$

Based on equation (30), \mathbf{H} can be represented by the eigenvalues and the left-eigenvectors without loss of generality, thus

$$\mathbf{H} = \mathbf{L}^{-1} \mathbf{\Lambda} \mathbf{L} \quad (35)$$

where $\mathbf{L}\mathbf{L}^{-1} = \mathbf{I}$. By substituting equation (35) into equation (34), we obtain

$$\frac{\partial \mathbf{U}}{\partial t} + \mathbf{L}^{-1} \mathbf{\Lambda} \mathbf{L} \frac{\partial \mathbf{U}}{\partial x} + \mathbf{S} = \mathbf{0} \quad (36)$$

By multiplying equation (36) with \mathbf{L} , we obtain

$$\mathbf{L} \frac{\partial \mathbf{U}}{\partial t} + \mathbf{\Lambda} \mathbf{L} \frac{\partial \mathbf{U}}{\partial x} + \mathbf{L}\mathbf{S} = \mathbf{0} \quad (37)$$

The evaluation of equation (37) at the boundary nodes are known as time-dependent compatibility conditions, C_{TD} , which is written as:

$$\mathbf{L} \left(\frac{\partial \mathbf{U}}{\partial t} + \mathbf{H} \frac{\partial \mathbf{U}}{\partial x} + \mathbf{S} \right) \Big|_{x=0,L} = 0 \quad (38)$$

and is expanded as follows

$$\begin{aligned} C_{TD} &= \left[-\frac{Q}{A} \pm \sqrt{\frac{K_p}{\rho} \left[\left(\frac{A}{A_0}\right)^{n_1} n_1 + \left(\frac{A}{A_0}\right)^{-n_2} n_2 \right]} \right] \frac{\partial A}{\partial t} \\ &+ \left[-\frac{Q}{A} \pm \sqrt{\frac{K_p}{\rho} \left[\left(\frac{A}{A_0}\right)^{n_1} n_1 + \left(\frac{A}{A_0}\right)^{-n_2} n_2 \right]} \right] \frac{\partial Q}{\partial x} \\ &+ \left[-\frac{Q^2}{A^2} + \frac{K_p}{\rho} \left[\left(\frac{A}{A_0}\right)^{n_1} n_1 + \left(\frac{A}{A_0}\right)^{-n_2} n_2 \right] \right] \frac{\partial A}{\partial x} \\ &+ \frac{2Q}{A} \frac{\partial Q}{\partial x} \\ &+ \left[\frac{K_p A}{\rho A_0} \left(-\left(\frac{A}{A_0}\right)^{n_1} n_1 - \left(\frac{A}{A_0}\right)^{-n_2} n_2 \right) \right] \frac{\partial A_0}{\partial x} \\ &+ \frac{A}{\rho} \left[\left(\frac{A}{A_0}\right)^{n_1} n_1 - \left(\frac{A}{A_0}\right)^{-n_2} n_2 \right] \frac{\partial K_p}{\partial x} + F_{\text{frict}} A = 0 \end{aligned} \quad (39)$$

The imposition of the compatibility conditions is accomplished by replacing the mass equation at the boundary nodes with equation (39). It should be noted that there are two opposite signs. The negative sign is applied at the inlet boundary while the positive sign is applied at the outlet boundary in accordance with the propagation of the outgoing characteristic waves so as to minimize the wave reflection at the boundaries as detailed in [5,6].

The first and second terms on the right hand side of equation (32) are referred as velocity, U and local wave speed of the nonlinear system, c , respectively which ratio is the speed index, S , introduced to describe the physiological flow in the stenotic vessel. Flow can be categorized as subcritical flow ($S < 1$), critical flow ($S = 1$) or supercritical flow ($S > 1$).

2.3 Validation of the Formulation

For validation purposes, a smooth stenosis previously studied in [3] is considered herein as shown in Figure 1 with the biological parameters as tabulated in Table 1. For comparison, results reported in [3] are extracted using WebPlotDigitizer.

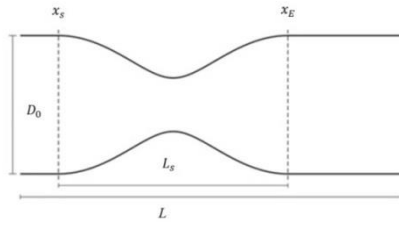


Figure 1 Smooth geometry of stenosis [3]

Table 1 Biological and geometrical parameters of stenosis [3]

Parameters	Values [Units]
Fluid density, ρ	995 kgm ⁻³
Fluid viscosity, μ	0.003Pa · s
Vessel stiffness, K_p	125 Pa
Tube law exponents, n_1	7
Tube law exponents, n_2	2.5
Nominal vessel diameter, D_0	0.006 m
Vessel radius, R	0.003 m
Length, L	0.03 m
Major laminar loss coefficient, f_L	20
Major separation loss coefficient, K_{sep}	0.2
Length of separation region, L_s	$2D_0$
Starting point for stenosis, x_s	$0.5D_0$
Ending point for stenosis, x_E	$2.5D_0$
Area reduction amplitude, λ_{A_0}	91.5%
Stiffness reduction amplitude, λ_{K_0}	10

2.3.1 Steady Case Validation

For the steady case, a constant inlet pressure of $P_1 = 100$ mmHg and a distal pressure of $P_2 = 60$ mmHg are applied. The external pressure P_e is fixed at zero so that the transmural pressure reflects the internal pressure within the blood vessel. λ_A and λ_K in equation (7) and equation (8) are given specifically for this case as:

$$\lambda_A(x) = \begin{cases} 1, & x < x_s \\ 1 - \lambda_{A_0} \sin^2 \left[\pi \left(\frac{x - x_s}{x_E - x_s} \right) \right], & x_s < x < x_E \\ 1, & x > x_E \end{cases} \quad (40)$$

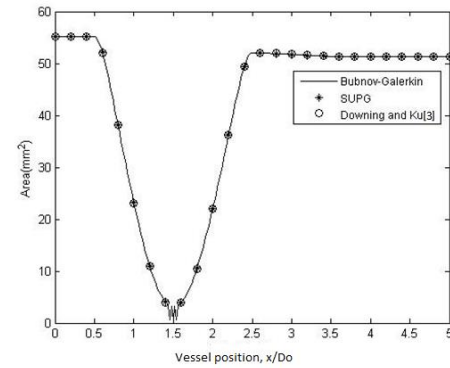
$$\lambda_K(x) = \begin{cases} 1, & x < x_s \\ 1 + \lambda_{K_0} \sin^2 \left[\pi \left(\frac{x - x_s}{x_E - x_s} \right) \right], & x_s < x < x_E \\ 1, & x > x_E \end{cases} \quad (41)$$

where x_s and x_E are the starting point and stopping point of the stenosis as illustrated in Figure 1. λ_{A_0} and λ_{K_0} are the area reduction amplitude and stiffness variation amplitude, respectively.

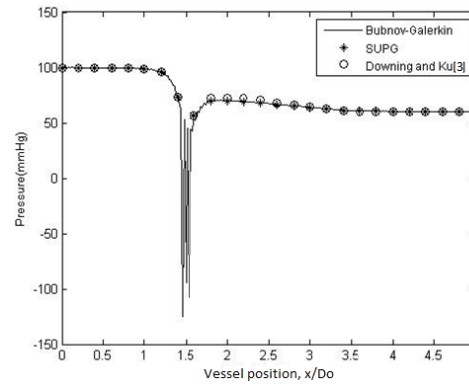
Bubnov-Galerkin finite element formulation is also run to highlight the occurrence of the oscillations at the

throat due to the lack of stabilization term. To note, Bubnov-Galerkin can be retrieved from the present SUPG formulation by simply eliminating the third integration term in equation (15). Numerical results obtained from both Bubnov-Galerkin and SUPG formulations are plotted and compared against the results of [3] in Figure 2. To note, in [3] the problem was solved using MacCormack finite difference approach.

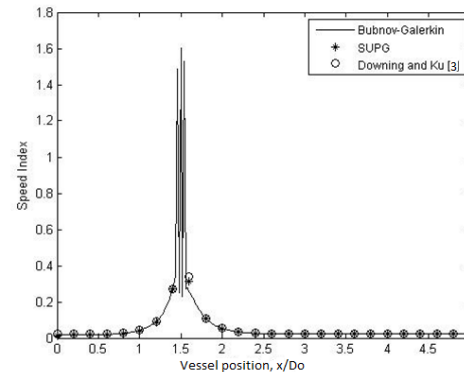
As expected, oscillations are observed for Bubnov-Galerkin in the throat region but vanished with the employment of the SUPG formulation. The numerical solutions have therefore been stabilized and validated against the numerical data of [3]. This marks our success in eliminating the oscillations through SUPG formulation.



(a) Cross Sectional Area



(b) Pressure



(c) Speed Index

Figure 2 Comparison of results of steady blood flow between Bubnov-Galerkin, SUPG and [3] for $P_2 = 60$ mmHg

2.3.2 Unsteady Case Validation

For the unsteady case, sinusoidal time varying term is added to the pressure at the inlet, given as

$$P_{in}(t) = 100 + 20 \sin(2\pi ft) \quad (42)$$

where f is the frequency. There are various outlet boundary conditions have been proposed in literature. Amongst others are the constant distal resistance and the Windkessel models [16]. In [3] the former model was employed. In this model, a time varying outlet pressure, $P_{ou}(t)$ with a constant distal resistance, R_{dis} is imposed. It is given as

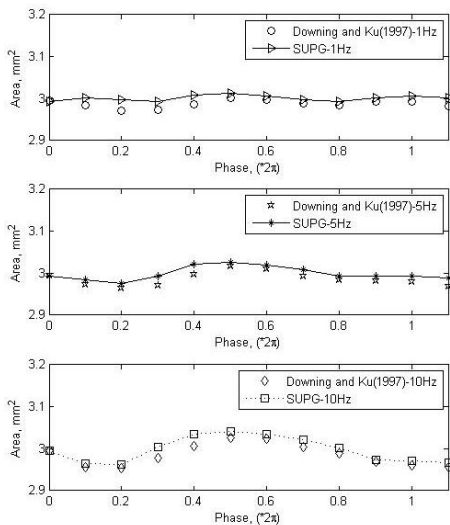
$$P_{ou}(t) = Q_{ou}(t)R_{dis} + P_{ven} \quad (43)$$

where P_{ven} is venous pressure having typical values in the range of 3 to 8 mmHg and $Q_{ou}(t)$ is given as

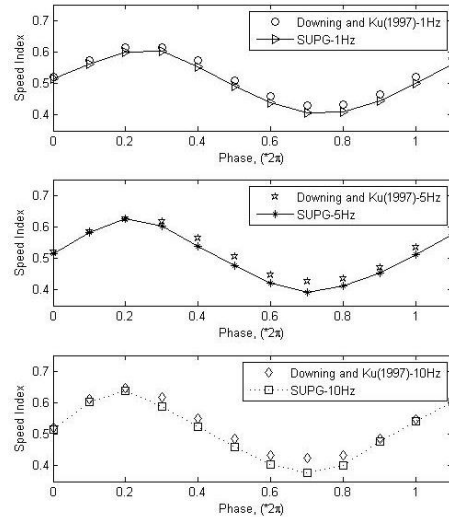
$$Q_{ou} = \left(\frac{Q_{ou} - Q_{ou-1}}{\Delta x} \right) \left(\frac{Q_{ou}}{A_{ou}} - \frac{Q_{ou-1}}{A_{ou-1}} \right) \frac{\Delta t}{2c} + Q_{ou-1} \quad (44)$$

where Q_{ou} and Q_{ou-1} are the flow rate at the outlet boundary node and at the adjacent node, respectively. The same subscript convention applies to A_{ou} .

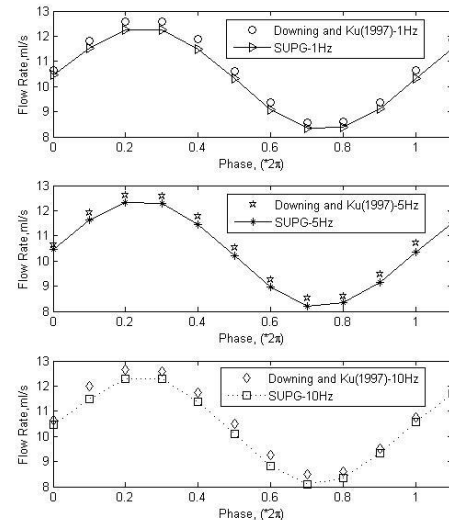
For this unsteady case, three different frequencies; 1 Hz, 5 Hz and 10 Hz, are evaluated. Steady solution obtained for $P_2 = 55$ mmHg is taken as the initial condition. $R_{dis} = 6.1$ mmHg/(ml/s) and $P_{ven} = 5$ mmHg are used in the calculation of the outlet pressure. Figure 3 shows the plots of the flow variables against cycle phase. SUPG are shown to agree well with the numerical data reported in [3]. With this validation we proceed to study the effect of the geometry of the stenosis to the flow characteristics in the next section.



(a) Minimum Cross Sectional Area



(b) Maximum Speed Index



(c) Average Flow Rate

Figure 3 Comparison of results between SUPG and [3] for $R_{dis} = 6.1$ mmHg/(ml/s) and $f = 1$ Hz, 5 Hz and 10 Hz

3.0 RESULTS AND DISCUSSION

3.1 Effect of Geometry of Stenosis

This section aims at investigating the effect of the geometry of stenosis to the flow characteristics and vessel collapse conditions. For this purpose, a hypothetical irregular shape of the stenosis is considered. The separation length of the stenosis is taken as $3D_0$. The irregular shape function, $\lambda_A(x)$ and the stiffness variation, $\lambda_K(x)$ of the blood vessel are respectively given in equation (45) and equation (46).

$$\lambda_A(x) = \begin{cases} 1, & x < x_s \\ 1 - \lambda_{A_0} \left(\frac{43}{100} \sin^2 \left[\pi \left(\frac{x - x_s}{x_E - x_s} \right) \right] + \frac{9}{13} \sin^2 \left[\frac{9}{2} \pi \left(\frac{x - x_s}{x_E - x_s} \right) \right] \right), & x_s < x < x_E - 0.3D_0 \\ 1 - \frac{43}{100} \lambda_{A_0} \sin^2 \left[\pi \left(\frac{x - x_s}{x_E - x_s} \right) \right], & x_s < x < x_E \\ 1, & x > x_E \end{cases} \quad (45)$$

$$\lambda_K(x) = \begin{cases} 1, & x < x_s \\ 1 + \lambda_{K_0} \left(\frac{43}{100} \sin^2 \left[\pi \left(\frac{x - x_s}{x_E - x_s} \right) \right] + \frac{9}{13} \sin^2 \left[\frac{9}{2} \pi \left(\frac{x - x_s}{x_E - x_s} \right) \right] \right), & x_s < x < x_E - 0.3D_0 \\ 1 + \frac{43}{100} \lambda_{K_0} \sin^2 \left[\pi \left(\frac{x - x_s}{x_E - x_s} \right) \right], & x_s < x < x_E \\ 1, & x > x_E \end{cases} \quad (46)$$

The baseline settings are, $\lambda_{A_0} = 85\%$, $\lambda_{K_0} = 10$ and $P_1 = 100$ mmHg. Cross sectional area along the vessel employing the shape function given by equation (42) is plotted in Figure 4 together with the smooth shape of equation (36). The minimum cross sectional area for smooth and irregular stenosis are 4.24 mm² and 4.41 mm², respectively which are located at $\frac{x}{D_0} = 2$ and $\frac{x}{D_0} = 2.14$, respectively. These cross sectional areas are also referred as no-flow minimum cross sectional areas. No-flow refers to the flow not driven by pressure gradient i.e. $P_1 = P_2$.

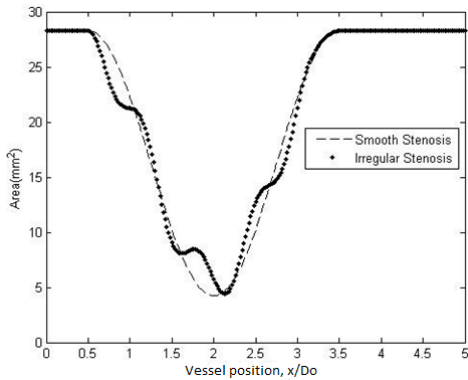
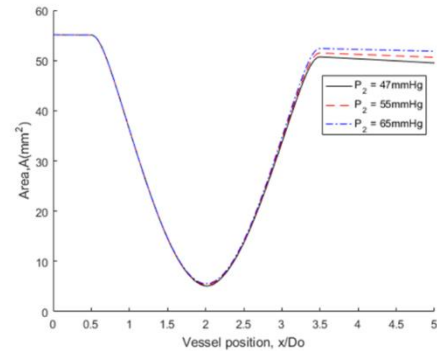


Figure 4 The initial cross sectional area for smooth and irregular stenosis with $\lambda_{A_0} = 85\%$

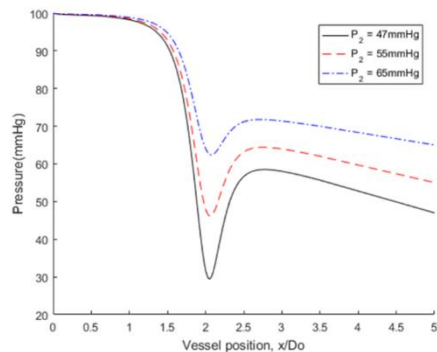
3.1.1 Steady Solutions

Distal pressure, P_2 is varied so as to observe the effects of geometry to the flow characteristics. Figures 5 and 6 show the results for three distal pressures; 47 mmHg, 55 mmHg and 65mmHg for smooth and irregular stenosis, respectively. The general trend is that the increase in the pressure gradient increases the speed of the flow (represented by the increased in speed index, S) and reduces the pressure inside the throat. For all conditions, flow is subcritical (i.e. $S < 1$) except for the case of irregular stenosis having distal pressure of 47 mmHg. In this case, the flow reaches supercritical and the corresponding pressure inside the throat

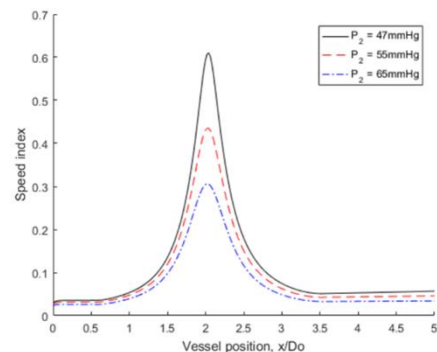
becomes negative. The latter indicates the collapse of the vessel.



(a) Cross Sectional Area



(b) Pressure



(c) Speed Index

Figure 5 Effect of distal pressure in smooth stenosis

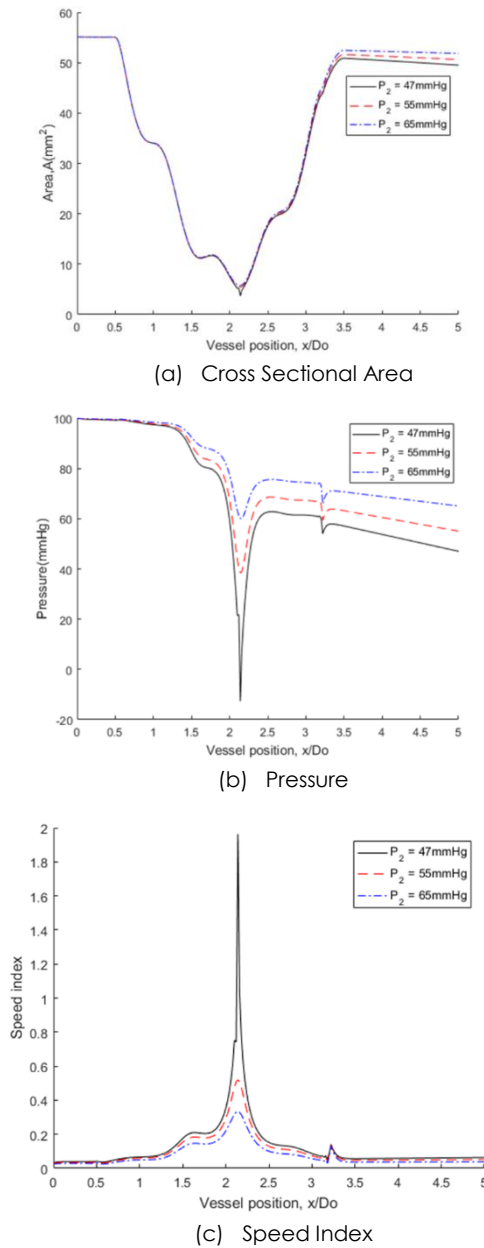


Figure 6 Effect of distal pressure in irregular stenosis

Figure 7 shows the results for other distal pressures given in the form of flow variables against pressure gradient, $(P_1 - P_2)$ mmHg. Continuous reduction in cross sectional area is observed in 7(a) for both smooth and irregular stenosis as the pressure gradient increases. Whilst the curve for smooth stenosis never passes its no-flow minimum cross-sectional area line, the irregular stenosis passes its line indicating collapse phenomenon. Similar trend is observed in 7(b) where the pressure curve of the irregular stenosis passes the x-axis and changes sign from positive to negative when smooth stenosis curve does not despite both are reducing. Inverse trend is observed in 7(c) where speed index increases with the increase in pressure gradient. However, flow in smooth stenosis remains subcritical.

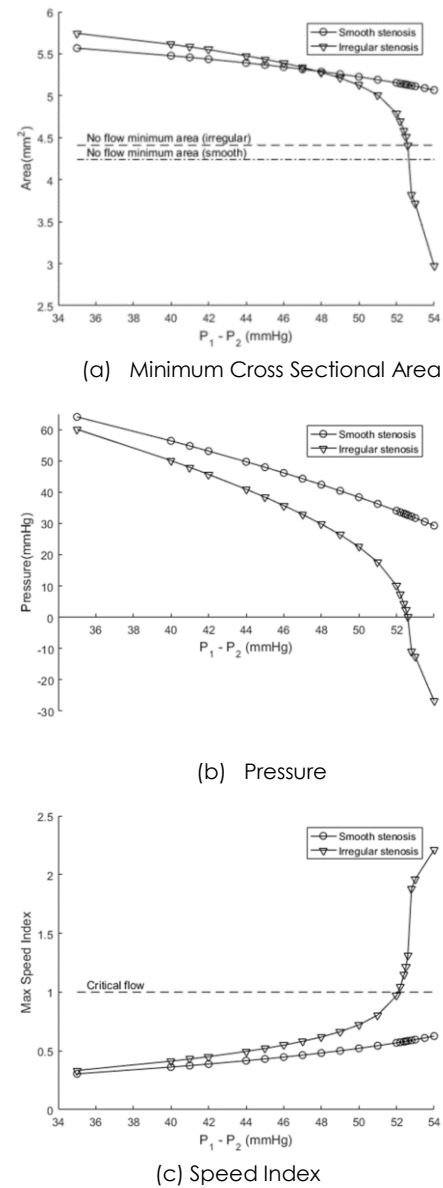


Figure 7 Plots of flow variables against pressure gradient

For irregular stenosis, supercritical flow is attained at pressure gradient of about 52 mmHg and beyond. For future reference, several numerical values of the flow variables are given in Tables 2 and 3 for smooth and irregular stenosis, respectively, taken at the location of the no-flow minimum cross-sectional areas.

Table 2 Numerical values of flow variables for smooth stenosis taken at $x/D_o = 2$

P_2 (mmHg)	A (mm ²)	P (mmHg)	S
46	5.07	29.28	0.63
47	5.11	31.71	0.60
49	5.19	36.23	0.54
51	5.26	40.41	0.50
52	5.29	42.38	0.48
53	5.32	44.28	0.46
55	5.37	47.95	0.43
60	5.48	56.36	0.36
65	5.57	64.02	0.30

Table 3 Numerical values of flow variables for irregular stenosis taken at $x/D_o = 2.14$

P_2 (mmHg)	A (mm ²)	P (mmHg)	S
46	2.97	-26.73	2.21
47	3.71	-12.66	1.96
49	5.01	17.61	0.80
51	5.21	26.38	0.66
52	5.28	29.78	0.62
53	5.34	32.85	0.58
55	5.44	38.39	0.52
60	5.61	50.07	0.41
65	5.74	60.07	0.33

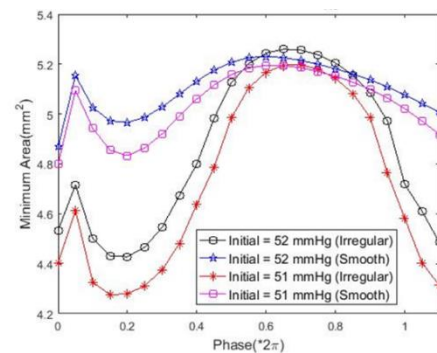
3.1.2 Unsteady Solutions

By imposing a time varying inlet pressure given by equation (42), we can observe the pulsatile behavior of the flow variables over time (or cycle phase). For this purpose, a frequency of 10 Hz is chosen and two initial conditions are selected for comparison. These are the data obtained from steady cases of 51 mmHg and 52 mmHg distal pressures. The former results in a distal resistance of 2.87 mmHg/(ml/s) for smooth stenosis and 2.55 mmHg/(ml/s) for irregular stenosis whilst the latter gives 2.97 mmHg/(ml/s) and 2.65 mmHg/(ml/s), respectively. Accordingly, these distal resistances and venous pressure of 3 mmHg are used in equation (43) for the determination of the outlet pressure. Figure 8 shows the plots of the flow variables against cycle phase. 8(a) shows that irregular stenosis is more deformable than the smooth stenosis as the cross sectional area fluctuation over the phase of the former is larger for a given initial condition. Such a larger fluctuation is also seen for other flow variables.

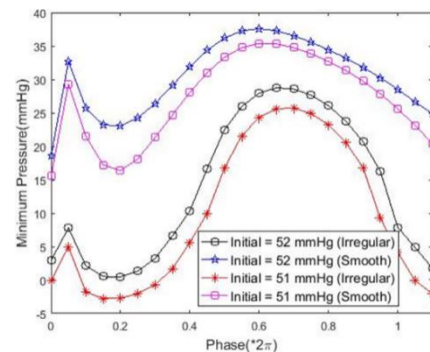
Collapse phenomenon is observed for irregular stenosis with 51 mmHg initial condition. Its cross sectional area becomes reduced from its no-flow minimum cross sectional area (i.e. 4.41 mm²) as the phase ranges from 0.08 to 0.32 during which the pressure becomes negative. The smallest cross sectional area attained by the curve is 4.27 mm² occurs at phase 0.17 accompanied by a negative pressure of (-) 2.83 mmHg. Although both curves of the irregular stenosis start off as supercritical which then transit into subcritical flows before half of the cycle (as

seen in 8(c)), initial condition of 52 mmHg could not bring down the pressure to negative values and the cross sectional area to be less than the no-flow minimum cross sectional area. This highlights that a supercritical flow is necessary but not sufficient for a vessel collapse.

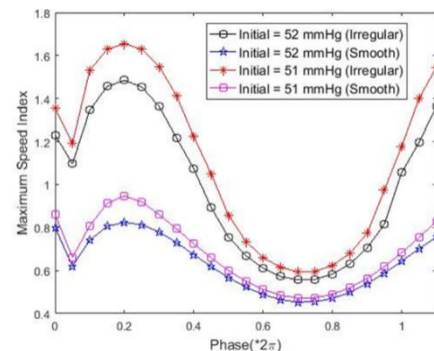
As in the steady case, no collapse phenomenon is observed for the smooth stenosis. Regardless of the initial conditions, the smallest cross sectional area and lowest pressure attained by the smooth stenosis is 4.8 mm² and 15 mmHg respectively, attained at the beginning of the cycle. The former is well above the no-flow minimum cross sectional area of 4.24 mm² and latter is far from becoming negative. The highest speed index is 0.95 just below the critical point. Flow in smooth stenosis is always subcritical.



(a) Minimum cross sectional area



(b) Minimum pressure



(c) Maximum speed index

Figure 8 Unsteady solutions for smooth stenosis

4.0 CONCLUSION

In this study, we have stabilized the solutions of an unsteady blood flow in stenosis from spurious oscillations by employing SUPG formulation. Our formulation has the advantage of allowing the interaction between the cross-sectional area, the volumetric flow rate and the pressure of the flow despite being one-dimensional. With such an advantage, we study the effect of the geometrical representation of the stenosis on the numerical solutions by comparing the results between a hypothetical irregular stenosis with a smooth stenosis under the same baseline conditions. After studying both steady and unsteady cases, we found that there are conditions when the two geometrical representations of the stenosis yield different flow characteristics. This, thus, highlights the importance of representing the shape of the stenosis as close as possible to render key information of the blood flow in during the modelling.

Acknowledgment

The authors owe much to the helpful suggestions and guidance of Professor John Ockendon of Oxford University at various stages of the work. The third author likes to thank Professor Abdul Rashid Abd Aziz and Dr Mohamed Latheef for the fruitful discussions he had at Universiti Teknologi PETRONAS.

References

- [1] Raghu, R. and Taylor, C. A. 2011. Verification of a One-dimensional Finite Element Method for Modeling Blood Flow in the Cardiovascular System Incorporating a Viscoelastic Wall Model. *Finite Elements in Analysis and Design*. 47(6): 586-592. <http://dx.doi.org/10.1016/j.finel.2010.12.012>.
- [2] Downing, J. M. 1995. Flow through a Compliant Stenotic Artery: A Parametric Evaluation. Armstrong Laboratory.
- [3] Downing, J. M. and Ku, D. N. 1997. Effects of Frictional Losses and Pulsatile Flow on the Collapse of Stenotic Arteries. *Journal of Biomechanical Engineering*. 119(3): 317-324. <http://dx.doi.org/10.1115/1.2796096>.
- [4] Ku, D. N., Zeigler, M. N. and Downing, J. M. 1990. One-dimensional Steady Inviscid Flow Through a Stenotic Collapsible Tube, *ASME Journal of Biomechanical Engineering*. 112: 444-450. <http://dx.doi.org/10.1115/1.2891209>.
- [5] Sochi, T. 2015. Navier-Stokes Flow in Cylindrical Elastic Tubes. *Journal of Applied Fluid Mechanics*. 8(2): 181-188.
- [6] Sochi, T. 2013. One-Dimensional Navier-Stokes Finite Element Flow Model. Imaging Sciences and Biomedical Engineering, King's College London, St Thomas' Hospital, London, England. <https://arxiv.org/abs/1304.2320>.
- [7] Sherwin, S.J., Formaggia, L., Peiró, J. and Franke, V. 2003. Computational Modelling of 1D Blood Flow with Variable Mechanical Properties and Its Application to the Simulation of Wave Propagation in the Human Arterial System. *International Journal for Numerical Methods in Fluids*. 43(6-7): 673-700. <http://dx.doi.org/10.1002/flid.543>.
- [8] Tang, A. Y., Mohd Noor, M. A., Mohd Yassin, A. Y. and Amin, N. 2017. One-Dimensional Fluid Structure Interaction (1D-FSI) Steady Flow Stable Formulation. *International Journal of Engineering Research & Technology*. 6(04): 1045-1055. <https://www.ijert.org/phocadownload/V6i4/IJERTV6IS040777.pdf>.
- [9] Johnston, P. R. and Kilpatrick, D. 1991. Mathematical Modelling of Flow Through An Irregular Arterial Stenosis. *Journal of Biochanics*. 24(11): 1069-1077. [https://doi.org/10.1016/0021-9290\(91\)90023-G](https://doi.org/10.1016/0021-9290(91)90023-G).
- [10] Andersson, H. I. Halden, R and Glamsaker, T. 2000. Effects of Surface Irregularities on Flow Resistance in Differently Shaped Arterial Stenoses. *Journal of Biomechanics*. 33(2000): 1257-1262. [http://dx.doi.org/10.1016/S0021-9290\(00\)00088-9](http://dx.doi.org/10.1016/S0021-9290(00)00088-9).
- [11] Chakrabarty, S., Mandal, P. K. and Sarifuddin. 2005. Effect of Surface Irregularities on Unsteady Pulsatile Flow in a Compliant Artery. *International Journal of Non-Linear Mechanics*. 40(2005): 1268-1281. <http://dx.doi.org/10.1016/j.jnonlinmec.2005.06.003>.
- [12] Norzieha, M., Mandal, P. K., Jonston, P.R. and Amin, N. 2009. A Numeric Simulation of Unsteady Blood Flow through Multi-irregular Arterial Stenoses. *Applied Mathematical Modelling*. 34(2010): 1559-1573. <https://doi.org/10.1016/j.apm.2009.09.008>.
- [13] Norzieha, M., Amin, N. Chakravarty, S. and Mandal, P. K. 2009. Unsteady Magneto-hydrodynamic Blood Flow through Irregular Multi-Stenosed Arteries. *Computers in Biology and Medicine*. 39(2009): 896-906. <https://doi.org/10.1016/j.compbiomed.2009.07.004>.
- [14] Sherwin, S. J., Franke, V., Peiró, J. and Parker, K. 2003. One-Dimensional Modelling of a Vascular Network in Space-time Variables. *Journal of Engineering Mathematics*, 47(3-4): 217-250. <http://dx.doi.org/10.1023/B:3AENGI.0000007979.32871.e2>.
- [15] Formaggia, L., Lamponi, D. and Quarteroni, A. 2003. One Dimensional Models for Blood Flow in Arteries. *Journal of Engineering Mathematics*. 47(3-4): 251-276. <https://doi.org/10.1023/B:ENGI.0000007980.01347.29>.
- [16] Du, T., Hu, D., Cai, D. 2015. Outflow Boundary Conditions for Blood Flow in Arterial Trees. *PLOS ONE*. 10(5): e012859. <https://doi.org/10.1371/journal.pone.0128597>.
- [17] Kolachalama, V. B., Bressloff, N. W., Nair, P. B. and Shearman, C. P. 2007. Predictive Haemodynamics in a One-dimensional Human Carotid Artery Bifurcation. Part I: Application to Stent Design. *IEEE Trans Biomed Eng*. 54(5): 802-812. <https://ieeexplore.ieee.org/document/4155000>.
- [18] Nisam, P. R., Binu, L. S. and Suresh, A. K. 2009. One Dimensional Modelling and Computation of Blood Flow and Pressure of a Stented Artery. *3rd International Conference on Bioinformatics and Biomedical Engineering*. 11-13 June 2009. Beijing, China, 1-5. <https://ieeexplore.ieee.org/document/5163145>.
- [19] Boileau, E., Nithiarasu, P., Blanco, P. J., Müller, L. O., Fossan, F. E., Hellevik, L. R., Donders, W. P., Huberts, W., Willemet, M. and Alastruey, J. 2015. A Benchmark Study of Numerical Schemes for One-dimensional Arterial Blood Flow Modelling. *International Journal for Numerical Methods in Biomedical Engineering*. 31(10): 1-33. <https://doi.org/10.1002/cnm.2732>.
- [20] Roy, M., Sikarwar, B. S., Bhandwal, M. and Ranjan, P. 2017. Modelling of Blood Flow in Stenosed Arteries. *Procedia Computer Science*. (115): 821-830. <https://doi.org/10.1016/j.procs.2017.09.164>.
- [21] Boileau, E., Nithiarasu, P., Blanco, P. J., Müller, L. O., Fossan, F. E., Hellevik, L. R., Donders, W. P., Huberts, W., Willemet, M. and Alastruey, J. 2015. A Benchmark Study of Numerical Schemes for One-dimensional Arterial Blood Flow Modelling. *Int. J. Numer. Meth. Biomed. Engng*. 31(10). <https://doi.org/10.1002/cnm.2732>.
- [22] Bessonov, N., Sequeira, A., Simakov, S., Vassilevskii, Y., and V. Volpert, V. 2016. *Math. Model. Nat. Phenom*. 11(1): 1-25. <https://doi.org/10.1051/mmnp/201611101>.
- [23] Soulaïmani, A. and Fortin, M. 1994. Finite Element Solution of Compressible Viscous Flows Using Conservative Variables.

Computer Methods in Applied Mechanics and Engineering. 118(3-4): 319-350.
[http://dx.doi.org/10.1016/0045-7825\(94\)90006-X](http://dx.doi.org/10.1016/0045-7825(94)90006-X).

[24] Donea, J., Huerta, A. 2003. *Finite Element Methods for Flow Problems*. England: John Wiley & Sons Ltd. 350.